Effect of Normal Breathing and Breath Holding on Seismocardiographic Signals and Heart Rate

T. Hassan[1], B. Rahman[1], R. H. Sandler[1,2] and H. A. Mansy[1,2]

1. Biomedical Acoustic Research Lab, University of Central Florida, Orlando, Florida, USA
2. Biomedical Acoustic Research Company, Orlando, Florida, USA
{thassan@knights., bnessa@knights., hansen.mansy@}ucf.edu, rhsandler@gmail.com

Abstract— Seismocardiography signals (SCG) are acoustic vibrations generated by heart activity and measured non-invasively on the surface of the chest. SCG may be used to diagnose and monitor cardiovascular conditions. The signal variability may limit the potentially high SCG clinical utility. It is known that breathing can cause variability, yet it is not well understood. The objective of this study is to quantify SCG and heart rate changes during normal breathing and breath holding (BH). Seismocardiography (SCG), electrocardiography (ECG), and airflow signals were recorded in eight healthy subjects during normal breathing and breath holding (at end inspiration and end expiration). The SCG events were detected and segmented. The heart rate was calculated using the R peak of ECG. Unsupervised machine learning (K-medoid clustering) was implemented using a dynamic time warping (DTW) distance to separate normal breathing SCG waveforms into two clusters. The SCG intra-group variability was calculated in the time domain. Normalized SCG energy in the 0-20 Hz range was also investigated. Results showed that the SCG average intra-cluster variability was 32% lower during breath holding compared to normal breathing. In addition, the average heart rate was 8% lower and normalized SCG energy was 9% lower in breath holding than normal breathing. Variable airflow and lung volume during normal breathing may cause these findings. SCG waveforms during breath holding can be more accurate due to the decreased variability. Hence, it may be useful to collect SCG during breath holding. The results of this study need to be verified with further investigation on a larger number of subjects.

I. Introduction

Seismocardiographic (SCG) signals are the vibrations of the chest wall that are developed because of the mechanical activity of the heart [1]. These vibrations are known to correlate with the mechanical processes surrounding the heart, which include valve closure, changes in blood momentum, and cardiac muscle contraction [2]–[6]. SCG can be measured non-invasively by placing an accelerometer on the surface of the chest. These signals can provide valuable information about heart function and can be potentially utilized to diagnose cardiac diseases. Previous studies have suggested the usefulness of different cardiac parameters, such as systolic time intervals and heart rate [2,4]. Currently, ECG is the most widely recognized method to measure cardiac activity. However, this signal is limited to the measurement of electrical myocardial activity. SCG can be used in conjunction with ECG to acquire information about both mechanical and electrical heart activity. In 2015, the leading global cause of mortality was heart disease. On average, someone in the United States dies of cardiovascular disease every 36 seconds [7]. From 2016 to 2017, the average annual direct and indirect cost of cardiovascular disease (CVD) in the United States was estimated to be 363.4 billion dollars [7]. Approximately 130 million adults in the US population (45.1%) are projected to have developed some form of CVD by 2035. The estimated total cost of CVD is expected to reach $1.1 trillion by 2035 [7]. In addition, an earlier study predicted that heart failure would increase by approximately 46% from 2012 to 2030 in adults [7]. SCG signals can be utilized as a noninvasive method for monitoring cardiovascular disease. SCG is believed to be associated with heart health and, hence, may be useful for monitoring cardiac conditions.

SCG waveform variability may interfere with extracting accurate waveforms, which can limit its clinical utility. The SCG utility can be increased if its variability is decreased and its sources of variability are better understood. One known source of variability is breathing. During breathing, there are changes in the heart position and pressure around the heart. These changes may introduce errors in the SCG interpretation yet may contain SCG morphological features of diagnostic value. Improved understanding of the sources of variability may help extract more accurate SCG waveforms and provide useful features that increase the diagnostic predictive value of SCG. To our knowledge, limited published information is available about SCG changes during BH. The purpose of this study is to quantify SCG and heart rate changes during regular breathing compared to BH. It is known that during BH some of the factors leading to the variability (such as the heart position) are nearly constant. Documenting SCG morphological changes under different breathing states may help enhance our understanding of SCG sources and suggest optimal breathing states and maneuvers for SCG recording.

II. Materials and Methods

Eight healthy subjects were recruited for our study after IRB approval. Subjects were asked to lay supine on a bed tilted to 45 degrees head facing forward with their feet extended horizontally. Figure 1 shows the methodology of our study.

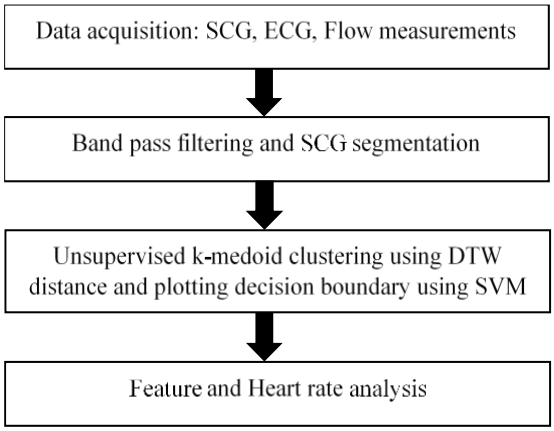

Figure 1. Methodology for acquiring and analyzing SCG

A. Data Acquisition

A biopotential recorder (IX-B3G, iWorx Systems, Inc., Dover, NH) was used to acquire the ECG signal. A tri-axial accelerometer (Model: 356A32, PCB Piezotronics, Depew, NY) was used to acquire SCG signals. The sensor was applied to the chest surface with double-sided medical grade tape on the 4th intercostal space near the left lower sternal border. A recent study [8]–[11] also used accelerometers to measure acoustic signals. A spirometer (Model: A-FH-300, iWorx Systems, Inc., Dover, NH) was used to measure the breathing flow rate. Figure 2 shows the experimental setup and sensor locations.

Subjects first rested for 2 minutes while breathing through a spirometer. The baseline tidal volume was measured during this time. Core signals (tri-axial SCG, ECG, and Spirometer flow rate) were collected for 5 minutes (while subjects maintained a tidal volume of +/- 20% of their baseline). End inspiration BH was done for 20 seconds (or as long as possible) while recording the signals, followed by a rest period of one minute. This cycle was repeated two more times (a total of 3 cycles for

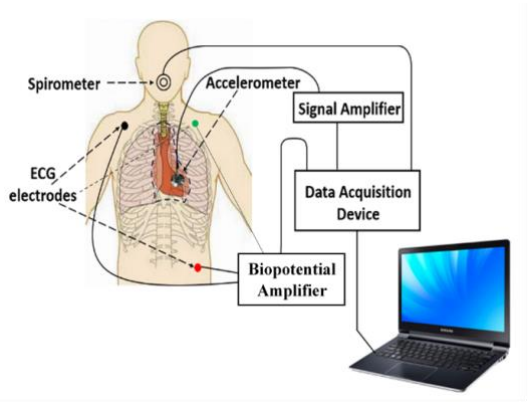

Figure 2. Sensor locations and experimental set up

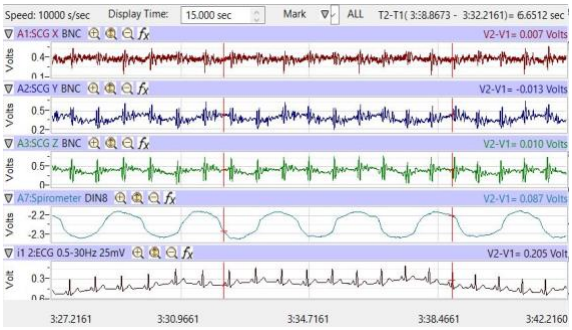

Figure 3. Raw data of SCG X, SCG Y, SCG Z, flow rate and ECG signals

end inspiration). Similarly, three trials of end expiration BH (20 seconds each, or as long as possible) were performed with 3 minutes of rest between trials. Figure 3 shows the raw data of triaxial SCG, ECG, and spirometer flow rate. Here, the sampling rate was 10,000 Hz.

B. Signal Processing

A band pass filter with a 0.05–200 Hz cut-off frequency was used to filter SCG signals after down sampling the signals to 1000 Hz. This is done to reduce background noise and baseline wandering due to respiration. Segmenting the SCG signal into SCG events (SCG signals during each heart cycle) was done using the R peaks of the simultaneously acquired ECG.

C. K-medoid Clustering

The SCG events were down sampled to 500 Hz before clustering. An unsupervised machine learning technique known as k-medoid clustering was used to cluster SCG events based on their morphology to reduce SCG variability during normal breathing. Here, dynamic time warping (DTW) distance was used to perform the clustering. This method of clustering time series based on waveform morphology was previously found to be more accurate than other methods [12].

DTW is a common measure of the similarity between two time series. The DTW algorithm exploits temporal distortions between two-time sequences to achieve an optimal global alignment [13,14]. Here, a measure of similarity is determined independently of the non-linear variations in time by "warping" the sequences in the time domain [13].

C1. DTW Procedure

Consider two time series $X = \{x_1, x_2, \ldots x_i, \ldots . x_n\}$ and $Y = \{y_1, y_2, \ldots y_j, \ldots . y_m\}$. The distance matrix is recursively filled by using Eq. 1:

$$D(i,j) = \delta(x_i, y_j) + min\begin{cases} D(i,j-1) \\ D(i-1,j) \\ D(i-1,j-1) \end{cases} \quad (1)$$

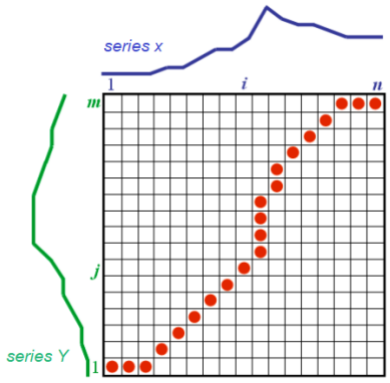

Figure 4. The optimal warping path between signals X and Y to illustrate DTW [13]

where $\delta(x_i, y_j) = (x_i - y_j)^2$ *or* $|x_i - y_j|$.

An optimal alignment $W = \{w_1, w_2, \ldots . w_k, \ldots, w_N\}$ is to be found where $w_k = (i, j)$ represents the alignment between i^{th} point of X and j^{th} point of Y. Figure 4 shows an illustration of a distance matrix and optimal wrapping path. Equation 2 calculates the optimal wrapping path.

$$DTW(X,Y) = argmin \sum_{k=1}^{k=N} D(w) \quad (2)$$

The K-Medoid clustering algorithm was implemented in MATLAB. Here, a representative event (medoid) is selected for the cluster instead of calculating a centroid for the cluster. Medoid is the event in the cluster that has the shortest distances to all other events. K-medoid clustering is advantageous over K-means clustering due to its low sensitivity to outliers [15].

C2. K-Medoid Algorithm

Step 1: Choose inputs: 1) Cluster number = K; 2) The SCG events $\{X_1, X_2, X_3, \ldots, X_i \ldots, X_N\}$ where *N* refers to the number of events and each event is a feature vector of signal amplitudes such that $X_i = \{x_1, x_2, x_3, \ldots, x_{l_i}\}$.

Step 2: Initialize the medoid for each cluster $C_1, \ldots, C_j, \ldots C_k$.

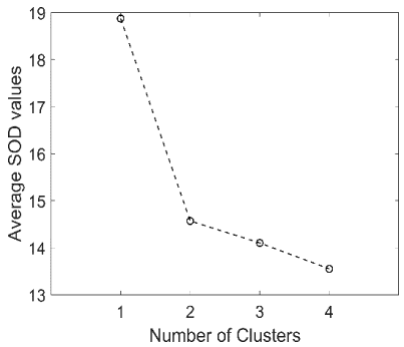

Figure 5. Average SOD for different number of clusters to illustrate elbow method

Step 3: For each SCG event, X_i, find the nearest cluster medoid C_j (using DTW as the distance measure) and assign X_i to cluster j.

Step 4: After assigning all events to a cluster, use Eq. 3 to update C_j based on the clustered events from the previous step:

$$C_j = argmin_{y \in \{X_{1j}, X_{2j}, \ldots, X_{ij}, \ldots, X_{nj}\}} \sum_{i=1}^{n_j} dtw(y, X_{ij}) \quad (3)$$

where X_{ij} is the i^{th} event of cluster j and n_j is the number of j events after step 2.

Step 5: Repeat steps 3 and 4 until cluster assignments do not change.

The optimal number of clusters was determined using the elbow method. Here, a small number of clusters were selected to optimize intra-cluster variance. Equation 4 calculates the average sum of distances (SOD) between each event and its cluster medoid, which measures intra-cluster variability.

$$SOD = \frac{1}{N} \sum_{j=1}^{k} \sum_{i=1}^{n_j} dtw(C_j, X_{ij}) \quad (4)$$

Here, N is the total number of events, X_{ij} is the i^{th} event for cluster medoid C_j, and n_j is the number of events for C_j.

Figure 5 shows the average SOD for the different numbers of clusters. Here, an elbow shape was observed when the number of clusters was 2, which is consistent with previous studies [16]–[18]. It can then be concluded that two clusters would lead to optimal intra-cluster variance with the fewest number of clusters.

D. Decision Boundary

After clustering, a decision boundary was calculated using a support vector machine (SVM) to show how accurately the two clusters are separated. The SVM algorithm maximizes the margin between two classes by finding a hyperplane for n features [19]. A decision boundary can be defined (for linearly separable data) as

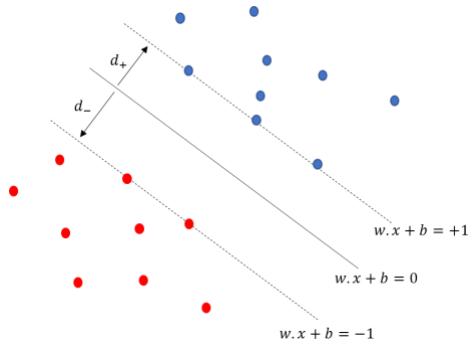

Figure 6. SVM hyperplane shows decision boundary and margin between the classes

$w.x_i + b = 0$ and the margins are defined using the hyperplanes $w.x_i + b = \pm 1$. Marginal data points on the boundary are known as the support vectors. Here, $w, x,$ and b are the weight vector, feature vector, and the bias, respectively. The aim of SVM is to maximize the decision margin $d = \frac{1}{\|w\|}$. SVM hyperplane and decision margin are illustrated in Figure 6.

III. Results and Discussion

Cluster distribution and decision boundary of SCG events are shown in the lung volume change vs flow rate plot for two subjects in Figure 7. The accuracy of the decision boundary was calculated using the following equation.

$$Accuracy = \frac{(TP+TN)}{(TP+FP+FN+TN)} \quad (5)$$

Figure 7 suggests that SCG clustering correlates with respiration, and the two clusters were well separated with high accuracy. Here, SCG events belonging to cluster 1 and cluster 2 are labeled as blue '∇' triangles and red 'o' circles, respectively. According to these findings, clusters are not separated based on respiratory flow rate

(a) Subject 1: Accuracy: 0.9750

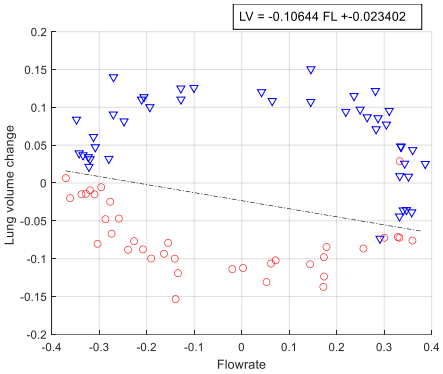

(b) Subject 2: Accuracy: 0.9851

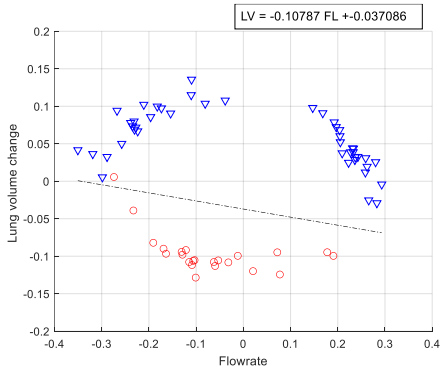

Figure 7. Cluster distribution on lung volume vs flow rate for 2 subjects of 1 minutes each.

Table 1. Intra-cluster variability change. The mean and standard deviation (SD) for the study subjects are listed. There was a drop with clustering ($p<0.05$) and an additional drop with breath hold ($p<0.05$).

Change in intra-cluster variability	Mean (%)	SD (%)
(After clustering -before clustering)/ before clustering	-20	9
(End inspiration- Normal breathing)/Normal breathing	-29	20
(End Expiration- Normal breathing)/Normal breathing	-35	19

(i.e., inspiration vs expiration phase) or by lung volume (i.e., high lung volume vs low lung volume). The clustering pattern was consistent for all study subjects.

A. Variability and Frequency Domain Features

The intra-cluster DTW distance was used to quantify how two waveform sets are not similar. Equation 6 calculates the intra-cluster variability using DTW distances:

$$Intra\text{–}cluster\ variability = \frac{1}{n_1+n_2}[\sum_{i=1}^{n_1} dtw(C_1, X_{i1}) + \sum_{i=1}^{n_2} dtw(C_2, X_{i2})]. \quad (6)$$

Here, X_{i1} and X_{i2} are the i^{th} SCG event of cluster 1 and cluster 2, respectively. C_1 and C_2 are the respective medoids of 2 clusters. n_1 *and* n_2 are cluster 1 and 2 total number of events, respectively. Relatively low intra-cluster DTW distance is indicative of well-separated groups.

Table 1 shows the change in intra-cluster variability between the un-clustered normal breathing, clustered normal breathing, BH end inspiration, and BH end expiration stats. Results showed an average 20% decrease ($p<0.05$) in variability for clustered normal breathing compared to un-clustered normal breathing. Also, it was found that there was an average 29% decrease ($p<0.05$) in variability for end inspiration and a 35% decrease ($p<0.05$) during end expiration, as compared to the clustered normal breathing state. The high SD is indicative of large inter-subject variability.

The energy of the SCG within the 0-20 Hz range was also analyzed, as previous studies suggested the utility of this feature. This energy was normalized by the energy in the 0-50 Hz range. Table 2 shows the change in normalized energy in the 0-20 Hz range. Results showed an average

Table 2. Change in normalized SCG energy in the 0-20 Hz band. The energy dropped with breath hold ($p<0.05$).

Change in the energy in the 0-20 Hz for all subjects	Mean (%)	SD (%)
(End inspiration BH- Normal breathing)/Normal breathing	-10	11
(End Expiration BH- Normal breathing)/Normal breathing	-8	11

10% decrease ($p<0.05$) during end inspiration BH and 8% decrease ($p<0.05$) during end expiration BH compared to normal breathing for all subjects.

B. Heart Rate

Heart rate during end inspiration BH, end expiration BH, and the 30 seconds before and after both BH was calculated and compared. Table 3 shows HR changes. Results showed that there was an average 9% and 11% decrease ($p<0.05$) in heart rate during end inspiration BH compared to before and after BH, respectively. Also, there was an average 5% and 7% decrease ($p<0.05$) in heart rate during end expiration BH compared to before and after BH, respectively.

Finally, spectral power in the 0.15–0.4 Hz range of the HRV was calculated, which is known as the high-frequency range (HF). Table 4 shows spectral energy changes in the HF range between the different breathing states. Results showed an average 58% decrease ($p<0.05$) in this energy during end inspiration BH and a 78% decrease ($p<0.05$) during end expiration BH compared to normal breathing. The reason for this decrease is likely because breathing frequency lies in this frequency range. Since the HRV associated with breathing (a phenomenon known as respiratory sinuous arrhythmia) is diminished with BH, lower variability is expected in this frequency band.

IV. Summary

In this paper, the SCG signal variability and heart rate during normal breathing and breath holding were investigated. Unsupervised machine learning was performed to cluster SCG signals acquired during normal breathing, which led to waveform variability reduction. The decision boundary was determined using a support vector machine, and classification accuracy was calculated. It was found that SCG waveforms could be separated into two groups with high levels of accuracy.

Table 3. Heart rate change. The heart rate decreased with breath hold ($p<0.05$).

Change in HR during BH for all subjects	Mean (%)	SD (%)
(End inspiration BH- before BH)/before BH	-9	6
(End inspiration BH- after BH)/after BH	-11	6
(End expiration BH- before BH)/before BH	-5	8
(End expiration BH- after BH)/after BH	-7	8

Table 4. Change in HRV energy in high frequency range (HF). There was a drop with breath holding ($p<0.05$).

Change in HF for all subjects	Mean (%)	SD (%)
(End inspiration BH-Normal)/Normal	-58	27
(End expiration BH-Normal)/Normal	-78	12

The changes in intra-cluster variability for un-clustered, clustered, and BH cases were analyzed. Results showed that there was a reduction in variability by 20% ($p<0.05$) after clustering and 32% ($p<0.05$) with BH. Heart rate and heart rate variability during BH were also compared with before and after BH. Results suggested that there was an 8% drop ($p<0.05$) in heart rate and a 68% drop ($p<0.05$) in heart rate energy in the 0.15-0.4 Hz range during BH cases. Limitations of the study include a small number of subjects and only one machine learning method was considered. In future studies, other unsupervised machine learning algorithms will be used to cluster SCG events during regular breathing, and other supervised classifiers will be used to calculate the decision boundary. The results will then be compared with the findings of this study. Also, future studies in a larger number of subjects are warranted to further verify these findings in healthy subjects and heart failure patients.

Acknowledgments

This material is based upon work supported by the National Science Foundation under Grant No. FW-HTF-P 2026516. The research reported in this publication was also supported by the National Heart and Lung Institute of the National Institutes of Health under award number R44 HL099053. Any opinions, findings, and conclusions or recommendations expressed in this material are those of the author(s) and do not necessarily reflect the views of the National Science Foundation or National Institute of Health.

COI statement: Richard H. Sandler and Hansen A. Mansy are part owners of Biomedical Acoustics Research Company, which is the primary recipient of the NIH grant R44HL099053, as such they may benefit financially as a result of the outcomes of the research work reported in this publication.

References

[1] B. S. Bozhenko, "Seismocardiography--a new method in the study of functional conditions of the heart," *Ter. Arkh.*, vol. 33, p. 55, 1961.

[2] D. M. Salerno, "Seismocardiography: A new technique for recording cardiac vibrations. concept, method, and initial observations," *J. Cardiovasc. Technol.*, vol. 9, no. 2, pp. 111–118, 1990.

[3] R. S. Crow, P. Hannan, D. Jacobs, L. Hedquist, and D. M. Salerno, "Relationship between seismocardiogram and echocardiogram for events in the cardiac cycle," *Am. J. Noninvasive Cardiol.*, vol. 8, pp. 39–46, 1994.

[4] K. Tavakolian, G. Portacio, N. Tamddondoust, G. Jahns, B. Ngai, G. Dumont, and A. Blaber, "Myocardial contractility: A seismocardiography approach," in *Engineering in Medicine and Biology Society (EMBC), 2012 Annual International Conference of the IEEE*, 2012, pp. 3801–3804.

[5] A. Taebi, "Characterization, Classification, and Genesis of Seismocardiographic Signals," Department of Mechanical and Aerospace Engineering, University of Central Florida, 2018.

[6] A. Taebi, R. H. Sandler, B. Kakavand, and H. A. Mansy, "Seismocardiographic Signal Timing with Myocardial Strain," in *Proceedings of the IEEE Signal Processing in Medicine and Biology Symposium (SPMB)*, 2017, pp. 1–2.

[7] S. Virani, A. Alonso, H. Aparicio, E. Benjamin, M. Bittencourt, C. Callaway, A. Carson et al., "Heart disease and stroke statistics—2021 update: a report from the American Heart Association," *Circulation*, vol. 143, pp. e254–e743, 2021.

[8] T. Hassan, L. Mckinney, R. Sandler, A. Kassab, C. Price, F. Moslehy and H. Mansy, "An Acoustic Approach for Detection of Developmental Dysplasia of Hip," in *Proceedings of the IEEE Signal Processing in Medicine and Biology Symposium (SPMB)*, Philadelphia, PA, 2018, pp. 1-6.

[9] T. Hassan, "Detection of DDH in Infants and Children Using Audible Acoustics," Department of Mechanical and Aerospace Engineering, University of Central Florida, Orlando, FL, 2019.

[10] T. Hassan, L. Mckinney, R. Sandler, A. Kassab, C. Price, F. Moslehy and H. Mansy, "A System for Measuring Sound Transmission Through Joints," in *Proceedings of the IEEE Signal Processing in Medicine and Biology Symposium (SPMB)*, Philadelphia, PA, USA, 2019, pp. 1-4.

[11] T. Hassan, R. Sandler, C. Price, A. Kassab and H. Mansy, "Detecting Hip Dysplasia Using Acoustic Excitation in a Pig Model," in *Proceedings of the IEEE Signal Processing in Medicine and Biology Symposium (SPMB)*, Philadelphia, PA, USA, 2020, pp. 1-3.

[12] J. Paparrizos and L. Gravano, "Fast and accurate time-series clustering," *ACM Trans. Database Syst.*, vol. 42, no. 2, p. 8, 2017.

[13] H. Sakoe and S. Chiba, "Dynamic programming algorithm optimization for spoken word recognition," *IEEE Transactions on Acoustics, Speech, and Signal Processing*, vol. 26, pp. 43-49, 1978.

[14] D. F. Silva and G. E. Batista, "Speeding up all-pairwise dynamic time warping matrix calculation," in *Proceedings of the 2016 SIAM International Conference on Data Mining*, 2016, pp. 837-845.

[15] J. Lei, "*An extended BIRCH-based clustering algorithm for large time-series datasets*," Dissertation, Department of Information and Communication Systems, Mid Sweden University, SE, 2017.

[16] P. Gamage, M. Azad, A. Taebi, R. Sandler, and H. Mansy, "Clustering Seismocardiographic Events using Unsupervised Machine Learning," in *Proceedings of the IEEE Signal Processing in Medicine and Biology Symposium (SPMB)*, Philadelphia, PA, USA, 2018.

[17] R. H. Sandler, T. Hassan, B. Rahman, N. Raval, R. J. Mentz, and H. A. Mansy, "Seismocardiographic Signal Variability During Regular Breathing and Breath Holding," *Journal of Cardiac Failure*, 2021.

[18] R. H. Sandler, T. Hassan, M. K. Azad, B. Rahman, N. Raval, R. J. Mentz, and H. A. Mansy, "Respiratory Phase Detection From Seismocardiographic Signals Using Machine Learning," *Journal of Cardiac Failure*, 2021.

[19] C. Cortes and V. Vapnik, "Support-vector networks," *Machine Learning*, vol. 20, no. 3, pp. 273-297, 1995.